# Lower Urban Humidity Moderates Outdoor Heat Stress

T. Chakraborty[1,2] , Z. S. Venter[3], Y. Qian[2] , and X. Lee[1]

[1]School of the Environment, Yale University, New Haven, CT, USA, [2]Pacific Northwest National Laboratory, Richland, WA, USA, [3]Terrestrial Ecology Section, Norwegian Institute for Nature Research—NINA, Oslo, Norway

**Abstract** Surface temperature is often used to examine heat exposure in multi-city studies and for informing urban heat mitigation efforts due to scarcity of urban air temperature measurements. Cities also have lower relative humidity, traditionally not accounted for in large-scale observational urban heat risk assessments. Here, using crowdsourced measurements from over 40,000 weather stations in ≈600 urban clusters in Europe, we show the moderating effect of this urbanization-induced humidity reduction on outdoor heat stress during the 2019 heatwave. We demonstrate that daytime differences in heat index between urban clusters and their surroundings are weak, and associations of this urban-rural difference with background climate, generally examined from the surface temperature perspective, are diminished due to moisture feedbacks. We also examine the spatial variability of surface temperature, air temperature, and heat index within these clusters—relevant for detecting hotspots and potential disparities in heat exposure—and find that surface temperature is a poor proxy for the intra-urban distribution of heat index during daytime. Finally, urban vegetation shows much weaker (~1/6th as strong) associations with heat index than with surface temperature, which has broad implications for optimizing urban heat stress mitigation strategies. These findings are valid for operational metrics of heat stress for shaded conditions (apparent temperature and humidex), thermodynamic proxies (wet-bulb temperature), and empirical heat indices. Based on this large-scale empirical evidence, surface temperature, used due to the lack of better alternatives, may not be suitable for accurately informing heat mitigation strategies within and across cities, necessitating more urban-scale observations and better urban-resolving models.

**Plain Language Summary** A central theme in urban climatology is that cities have higher air temperature, and thus higher potential for heat stress, than their background rural landscapes. Due to limitations in observation and modeling, surface temperature is often used as a proxy for urban heat stress. However, surface temperature is not air temperature and several other factors contribute to heat stress. It is critical to know how well, if at all, surface temperature can capture the potential for urban heat stress, which has been traditionally difficult to measure using ground observations due to data scarcity. We use measurements from over 40,000 citizen weather stations over Europe to address this important gap and compare distributions of satellite-derived surface temperature, air temperature, and heat indices during the July 2019 heatwave. We find that lower relative humidity due to urbanization partly offsets the effect of higher air temperatures and thus moderates the potential for urban heat stress. Moreover, satellite-derived surface temperature shows very weak relationships with air temperature and heat index, both within cities and when examining urban-rural differences across cities. Finally, urban vegetation is much less effective at reducing heat index than at reducing surface temperature. These results are relevant for informing future urban research and heat mitigation efforts.

## 1. Introduction

As the world continues to warm, with heatwaves becoming more frequent and intense (Perkins-Kirkpatrick & Lewis, 2020), urban areas are expected to face the brunt of the impacts due to large populations and higher temperatures (Heaviside et al., 2017; Heilig, 2014). That cities, on average, are warmer than their surroundings—the urban heat island (UHI) effect—is well-established (Arnfield, 2003; Qian et al., 2022). However, the temporal pattern and magnitude of this phenomenon varies substantially across cities and depends on the type of temperature measurement (Ho et al., 2016; Venter et al., 2021; Zhang et al., 2014). Traditionally, the UHI intensity was quantified using in situ air temperature ($T_a$) measurements (Howard, 1833). However, many recent large-scale observational and modeling studies on the UHI, and urban climate in general, have focused on radiative skin or surface temperature ($T_s$) (Chakraborty & Lee, 2019; Chakraborty et al., 2019; Clinton & Gong, 2013; Hoffman et al., 2020; Hsu et al., 2021; L. Zhao et al., 2014, 2017; Manoli et al., 2019; Mentaschi et al., 2022; Schwaab et al., 2021), with many of these studies commenting on heat exposure in cities, their public health consequences,

**Validation:** T. Chakraborty
**Visualization:** T. Chakraborty
**Writing – original draft:** T. Chakraborty
**Writing – review & editing:** T. Chakraborty, Z. S. Venter, Y. Qian, X. Lee

and potential mitigation strategies. Similarly, maps made from satellite-derived $T_s$ are often used as a guide for planning heat mitigation strategies by decision makers (Keith et al., 2019). However, $T_a$ is more relevant for heat exposure than $T_s$, but is difficult to measure in cities due to the dearth of standard weather stations and hard to model due to multiple confounding factors (Hardin et al., 2018; Ho et al., 2016; Muller et al., 2013; Stone et al., 2019). The two variables—$T_a$ and $T_s$—are physically distinct (Jin & Dickinson, 2010), and the urban-rural differences in $T_a$ ($\Delta T_a$; also called canopy urban heat island; CUHI) and $T_s$ ($\Delta T_s$; also called surface urban heat island; SUHI) are also not well-correlated, especially during the day (Du et al., 2021; Venter et al., 2021; Zhang et al., 2014). This daytime decoupling between CUHI and SUHI brings into question the potential public health and policy implications of $T_s$-based urban studies.

Urban areas may also be drier than their surroundings (particularly in humid climate) due to the removal of vegetation and pervious surfaces—the urban dry island (UDI) effect (Lokoshchenko, 2017; Qian et al., 2022). The human physiological response to heat depends not just on $T_a$, but also on relative humidity (RH) (Anderson et al., 2013; Raymond et al., 2020; Sherwood & Huber, 2010). In comparison to the multitude of studies on the UHI, the UDI is rarely considered in large-scale urban heat risk assessments due to the lack of consensus on a standard metric for urban moisture content (Wang et al., 2021) and the difficulty in measuring near-surface moisture within cities, even when using satellites. Electricity demand for cooling buildings, expected to be enhanced due to the UHI, also depends on atmospheric humidity (Maia-Silva et al., 2020). Therefore, a more accurate understanding of the impact of urbanization on public health, energy demand, and the economy should account for the combined impacts of $T_a$ and RH. Although modeling studies have the freedom to examine simulated $T_a$ and RH (and thus, potential for heat stress) over urban areas (Huang et al., 2021; L. Zhao et al., 2021; Oleson et al., 2015; Sarangi et al., 2021), models have simplified urban representations with multiple sources of uncertainty (Krayenhoff et al., 2021; Qian et al., 2022; Sharma et al., 2021; Zheng et al., 2021). Additionally, it is computationally expensive to run such models at fine-enough scales to resolve intra-urban variability.

Here, we combine dense citizen weather station (CWS) measurements and satellite observations over Europe during the July 2019 heatwave to comprehensively examine the distributions of $T_s$, $T_a$, RH, and potential for outdoor heat stress within and across satellite-derived urban clusters. We consider several metrics, both empirical and thermodynamic, for estimating potential for heat stress. The primary metric considered is the apparent temperature ($HI_0$) used by the US National Weather Service (NWS), which describes what the temperature feels like to humans under shade when humidity is accounted for (Rothfusz, 1990; Steadman, 1979). Our results, based on measurements from over 40,000 (after quality control) CWSs in over 600 clusters, suggest that the lower RH in these cities partially cancels out the impact of higher $T_a$ on moist heat stress during daytime, resulting in smaller differences in $HI_0$ (and several other heat indices considered) between urban areas and their surroundings. We also analyze the spatial gradients of these variables within clusters and demonstrate that satellite-derived $T_s$ poorly captures the spatial distribution of ambient $HI_0$ within cities. Finally, with reference to the notion of employing urban vegetation to reduce local-scale heat stress, we find that vegetation is much less efficient at lowering $HI_0$ than lowering $T_s$ at these scales. These results demonstrate the contrasting roles $T_a$ and RH play to moderate urbanization-induced $HI_0$ across scales during a heatwave period—the most comprehensive analysis of this sort using in situ observations—and suggest that we need to re-evaluate the current dependence on satellite-derived insights for urban design and policy making.

## 2. Methods

### 2.1. Urban Clusters and Their Rural Backgrounds

Urban clusters over Europe are the primary regions of interest for our analysis. These clusters were generated by vectorizing contiguous $1 \times 1$ km pixels classified as either low- or high-density urban in the Global Human Settlement Layer's (GHSL) settlement classification data set (version R2016A) (Pesaresi & Freire, 2016). The GHSL layer detects urbanization using the spectral signature of built-up surfaces measured by satellites and has been used to generate similar urban clusters in other parts of the world (Chakraborty et al., 2021). Since many of these clusters are small and do not have enough CWS observations, clusters smaller than the 50th percentile of the urban cluster area distribution are removed, leaving 929 clusters (Figure 1a).

The rural or background reference for each cluster is a polygon buffer of 10 km width surrounding it (Figure 1b), a definition of rural reference that has been used in the past (Clinton & Gong, 2013). Since some urban clusters are
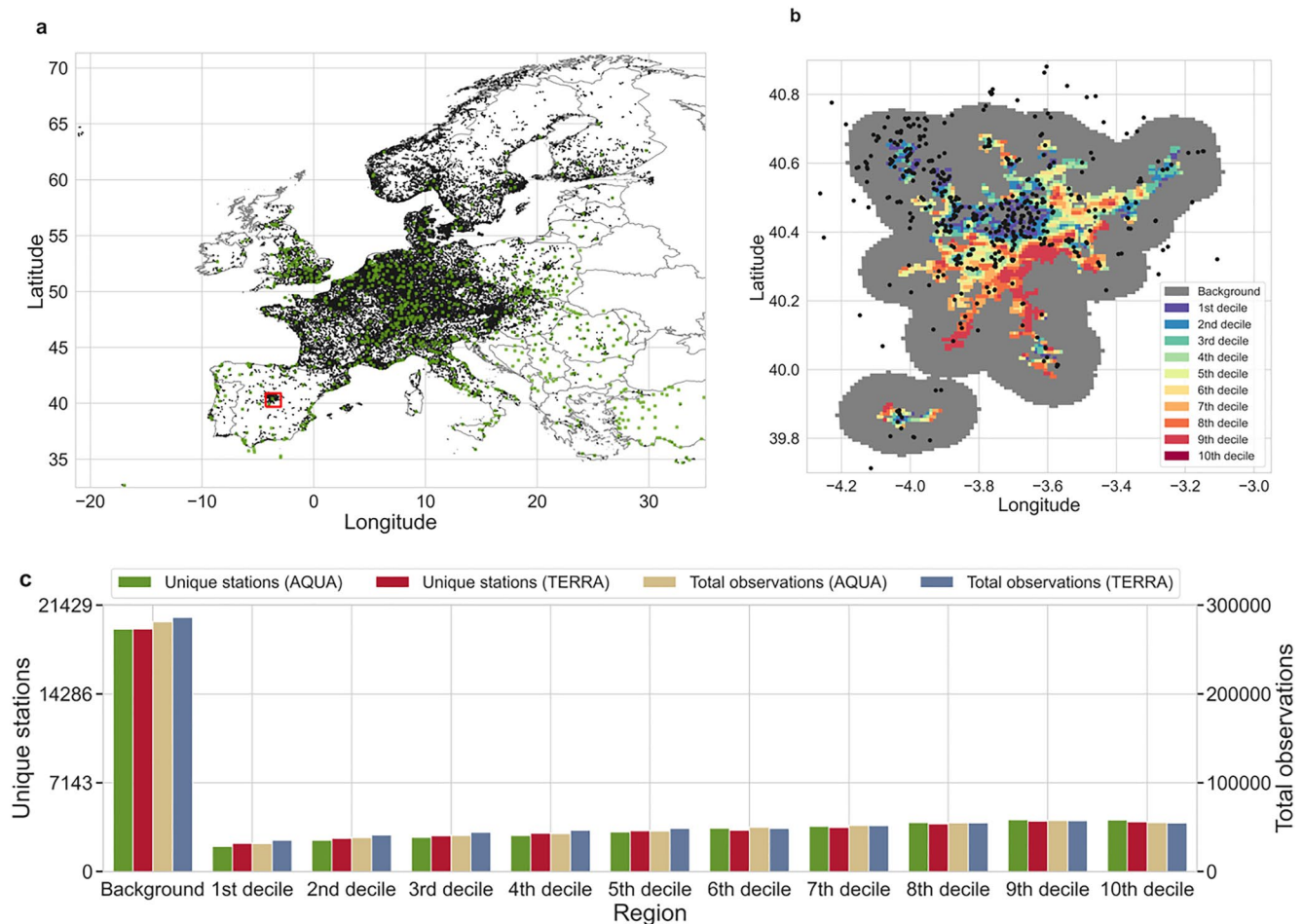
**Figure 1.** Regions of interest and data summary. Panel (a) shows the spatial distribution of Netatmo stations (black dots) over Europe during the heatwave of July 2019, as well as the urban clusters (in green) in the region. Panel (b) shows an example of the daytime ($\approx$1:30 p.m.) surface temperature ($T_s$) decile neighborhoods (from up to 10th to 90th–100th percentile) within the urban cluster of Madrid, Spain (see the red box in panel (a) for location) based on daily Moderate Resolution Imaging Spectroradiometer Aqua scenes. Similar regions are created corresponding to Terra observations (not shown). The black dots show the Netatmo stations over the cluster and the gray region represents the rural reference. Panel (c) shows the total number of valid observations and unique stations for each region that correspond to the Terra and Aqua overpass times.

closer to each other than 20 km, a focal mode smoothing function is applied to prevent any overlap between the rural references of nearby clusters. This function designates a border between two overlapping buffers such that they are equidistant to the original urban clusters they surround. More information about the generation of the urban clusters and their rural references can be found in Venter et al. (2021).

## 2.2. Citizen Weather Station Data

All hourly $T_a$ and RH observations from CWSs over Europe were downloaded for July 2019 from Netatmo (https://netatmo.com/). This data set includes measurements from 113,215 stations during this period. CWS data have errors and biases related to less-than-ideal sensor placement, insufficient site metadata, lack of radiation shield, and instrumental errors (Meier et al., 2017). We follow a quality-control procedure developed for these sensors using the "Crowd-QC" package in R (Napoly et al., 2018). The quality-control procedure starts with removal of statistical outliers using a modified z-score approach and the hourly $T_a$ distributions. Then, sites for which the measured $T_a$, when correlated against the spatial median of monthly $T_a$, show Pearson's correlation coefficients less than 0.9, are removed. These steps reduce the number of available stations to 95,084.

Since we wanted to get representative values for July 2019, we also removed Netatmo stations with more than 20% missing data during this period, leaving 75,293 stations. This threshold was found sufficient to capture the

monthly climatological state in a previous study (Venter et al., 2021). We note that most of the quality-control procedure has been developed for $T_a$, not RH. However, since the Netatmo sensor module houses both $T_a$ and RH sensors, issues related to sensor misplacement and instrumental errors would also minimize large errors in measured RH. This is also confirmed through validation of the CWS measurements (see corresponding subsection below).

### 2.3. Calculating Apparent Temperature and Other Heat Indices

Since humans primarily thermoregulate through sweating, the moisture content of the air limits our body's ability to dissipate heat, making it an important factor in addition to $T_a$ when studying potential for heat stress (Sherwood & Huber, 2010). There are multiple metrics of heat stress that account for moisture. Here, we use the heat index used by the US NWS, also known as apparent temperature. This index ($HI_0$) is calculated in multiple steps. We start with a simple formula whose results are consistent with those from Steadman (1979):

$$HI_0 = 0.5 \times [T_a + 61 + [(T_a - 68) \times 1.2] + (0.094 RH)] \tag{1}$$

where $T_a$ is in °F and RH is in percentage. If the average of $T_a$ and this heat index is less than 80°F, this is the final equation used. If the average is equal to or above 80°F, the Rothfusz regression (Rothfusz, 1990) is used instead, given by

$$HI_0 = -42.379 + 2.04901523 T_a + 10.14333127 RH - 0.22475541 T_a RH - 6.83783$$
$$\times 10^{-3} T_a^2 - 5.481717 \times 10^{-2} RH^2 + 1.22874 \times 10^{-3} T_a^2 RH + 8.5282 \tag{2}$$
$$\times 10^{-4} T_a RH^2 - 1.99 \times 10^{-6} T_a^2 RH^2$$

Similar to Equation 1, the $T_a$ is input in °F. Additional adjustments are made for low and high values of RH, consistent with the method used in operational heat warning systems by the US NWS (Rothfusz, 1990).

To check the consistency of our results, we also consider several other empirical approximations of moist heat stress that combine the impact of $T_a$ and moisture, including the humidex (Masterton & Richardson, 1979) and one of each functional forms of the heat index approximation in °C reviewed in Anderson et al. (2013).

The humidex can be expressed as

$$\text{Humidex} = T_a + 0.5555 \times \left( 6.11 \times e^{5417.753 \times \left( \frac{1}{273.16} - \frac{1}{273.15 + T_D} \right)} - 10 \right) \tag{3}$$

where $T_D$ is the dew-point temperature in °C and is given by

$$T_D = \frac{243.04 \times \left\{ \ln\left(\frac{RH}{100}\right) + \frac{17.625 \times T_a}{243.04 + T_a} \right\}}{17.625 - \left\{ \ln\left(\frac{RH}{100}\right) + \frac{17.625 \times T_a}{243.04 + T_a} \right\}} \tag{4}$$

Finally, the other four functional forms of the heat index considered here are denoted by $HI_1$, $HI_2$, $HI_3$, and $HI_4$ and are given by

$$HI_1 = T_a - 1.0799 e^{0.03755 T_a} \left( 1 - e^{0.0801(T_D - 14)} \right) \tag{5}$$

$$HI_2 = -2.653 + 0.994 T_a + 0.0153 T_D^2 \tag{6}$$

$$HI_3 = -8.7847 + 1.6114 T_a - 0.012308 T_a^2 + RH \left[ 2.3385 - 0.14612 T_a + \left( 2.2117 \times 10^{-3} \right) T_a^2 \right]$$
$$+ RH^2 \left[ -0.016425 + \left( 7.2546 \times 10^{-4} \right) T_a + \left( -3.582 \times 10^{-6} \right) T_a^2 \right] \tag{7}$$

$$HI_4 = T_a - 0.55 \times (1 - 0.001 RH)(T_a - 14.5) \tag{8}$$

In addition to these heat indices, we also calculate the wet-bulb temperature ($T_w$), a thermodynamic measure of how effectively humans can cool down via sweating (Sherwood & Huber, 2010) and a metric for heat stress often used in climate-related studies (L. Zhao et al., 2021; Mishra et al., 2020; Raymond et al., 2020), using the formulation proposed by Stull (2011). The results for $T_w$ remain the same when using an iterative calculation method (not shown). Note that all the metrics for heat stress examined here refer to outdoor conditions. Additionally, these metrics, being functions of only $T_a$ and RH, are only valid when one is under shade. The results of the study should be interpreted keeping this in mind.

## 2.4. Research-Grade Weather Station Data

To evaluate the CWS measurements, we acquired observations from the European Climate Assessment & Dataset (ECA&D) weather stations (ECA&D, 2013) for July 2019. The ECA&D data set provides daily observations from meteorological stations throughout Europe. We extract daily $T_a$ and RH from this network and calculate $HI_0$ using Equations 1 and 2.

## 2.5. Reanalysis Data

We also extract hourly and monthly $T_a$, $T_D$ (RH is not provided by this data set), surface pressure, and accumulated precipitation from the ECMWF (European Centre for Medium-Range Weather Forecasts) Reanalysis 5th Generation Land (ERA5-Land) data set (Muñoz-Sabater et al., 2021). The ERA5-Land provides surface variables at high (≈9 km) resolution and is based on the tiled ECMWF Scheme for Surface Exchanges over Land incorporating land surface hydrology (H-TESSEL) and is constrained by multiple observational data sets (Muñoz-Sabater et al., 2021). The hourly RH is computed by dividing the saturation vapor pressure ($e_s$) at $T_D$ by the saturation vapor pressure at $T_a$, both calculated using the August-Roche-Magnus approximation (Alduchov & Eskridge, 1996). Thus,

$$RH = 100 \times \frac{e_s(T_D)}{e_s(T_a)} \tag{9}$$

$$e_s(T) = 6.1094 e^{\left(\frac{17.625T}{T+243.04}\right)} \tag{10}$$

where $T$ is the temperature (either $T_a$ or $T_D$) in °C.

## 2.6. Validating Citizen Weather Station Data

Since the ECA&D weather stations are generally not set up in cities, we start by matching each ECA&D station with rural Netatmo stations that are within a buffer of 2,000 m. Some of the ECA&D stations have daily mean RH of 100% for almost the entire month, which is physically implausible. These are removed from the analysis. For each day that measured $T_a$ and RH are available for a valid ECA&D station, we choose the corresponding Netatmo stations that include all 24 hr of observations to reliably compute the daily means. The composite means for the whole period (July 2019) from ECA&D and the Netatmo sensors are then correlated (Figures 2a–2c). A few of the Netatmo sensors show implausibly large differences in mean daily $T_a$ (>10°C) from the corresponding ECA&D measurements. To account for this in a statistically robust manner, we remove Netatmo stations whose difference in measured $T_a$ and RH with its nearby ECA&D station is above 99 percentile or below 1 percentile of the whole distribution. These stations are not used for any of the subsequent analyses. Similar evaluations are difficult to perform for urban Netatmo stations at these scales. Even when weather stations are available in cities, they are usually not in residential areas like most of the Netatmo stations. Standard "urban" weather stations are usually at nearby airports, and thus do not usually reflect the outdoor exposure conditions of the average urban resident. However, since the sensors used in the Netatmo stations have standardized specifications, we expect the weather stations within cities to perform similarly barring systemic placement errors.

Overall, the CWS-measured $T_a$ and RH show strong correlations (particularly for $T_a$) with ECA&D observations ($r^2$ = 0.8 and 0.53, respectively; Figures 2a and 2b) during this period. The root-mean-square-error (RMSE) and mean bias error (MBE) are both reasonably small (RMSE = 1.85°C and MBE = 1.63°C for $T_a$; 5.47% and −2.82% for RH). The Netatmo sensors overestimate $T_a$ and underestimate RH, which would be expected if they
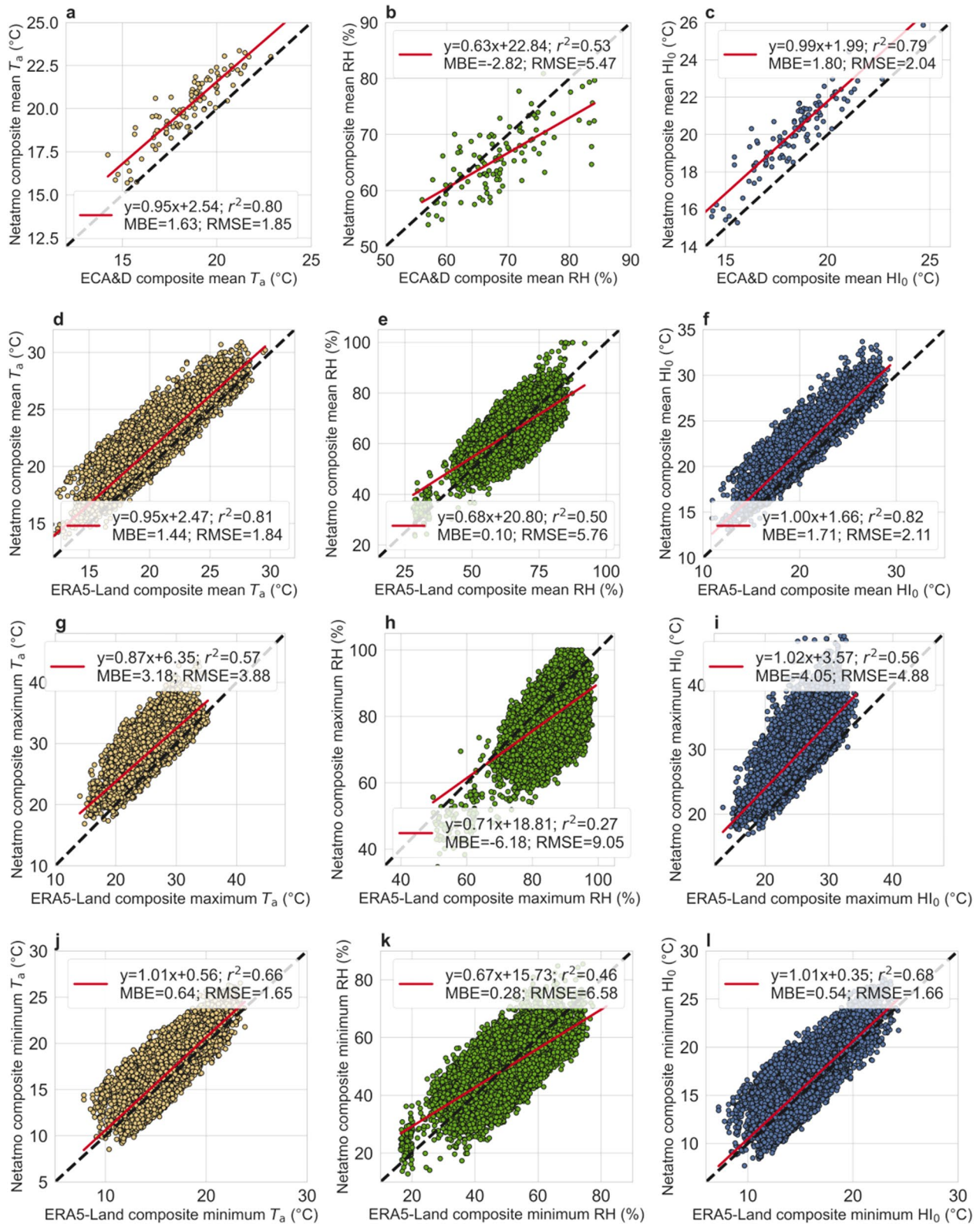
**Figure 2.** Validation of citizen weather station data. Composite mean Netatmo (a) air temperature ($T_a$), (b) relative humidity (RH), and (c) heat index ($HI_0$) against corresponding European Climate Assessment & Dataset (ECA&D) weather stations for the whole study period (July 2019). Panels (d–l) show composite mean (d–f), maximum (g–i), and minimum (j–l) Netatmo observations against corresponding ECMWF (European Centre for Medium-Range Weather Forecasts) Reanalysis 5th Generation Land (ERA5-Land) gridded values. Each dot represents a composite value and the corresponding metrics for evaluation are shown in the legend.

lack radiation shields (Da Cunha, 2015). However, the distribution of $HI_0$ is well captured by these sensors (Figure 2c).

The use of daily mean values for evaluation would underestimate the biases caused in sun-exposed sensors due to the absence of radiation shields during daytime. Although the ECA&D data set includes maximum and minimum $T_a$ for each station, it only includes daily mean RH, which would not allow us to calculate the maximum and minimum $HI_0$. Instead, we use the maximum and minimum composite values (in addition to daily means) from ERA5-Land data to compare against the corresponding rural Netatmo measurements (Figures 2d–2l) after removing daily differences greater than 99 percentile and less than 1 percentile of the distribution. Consistent with the comparisons with ECA&D, the Netatmo measurements overestimate $T_a$ and $HI_0$ (Figures 2d and 2f). The maximum composite $T_a$, which would be generally in the early afternoon (Figure S1a in Supporting Information S1), is overestimated more (MBE = 3.18°C) than the mean composite $T_a$ (MBE = 1.44°C). For minimum values, generally during early morning, the biases are much smaller with even smaller biases for $HI_0$ (Figure 2l). For all cases, there is compensation between the biases due to $T_a$ and RH, leading to slopes closer to 1 for $HI_0$ than for $T_a$. Additionally, the evaluations for RH show slope coefficients less than 1 with the Netatmo observations overestimating RH (or showing less underestimation) in drier conditions compared to the reference data (Figures 2b, 2e, 2h and 2k). This has implications for our results since urban areas, being drier, may not be dry enough (compared to the rural reference) according to the Netatmo measurements. As such, the compensating effect of urbanization-induced drying seen here may be underestimated.

Note that the larger spread between the ERA5-Land and Netatmo is expected since these estimates are at different scales. A Netatmo measurement represents information for a small footprint around the CWS, while the ERA5-Land estimate is for $a \approx 9$ km grid overlaying that Netatmo site. Although there are biases between the Netatmo data and the point and gridded estimates, the distributions are captured well by the CWSs, particularly for $T_a$ and $HI_0$, with slopes close to 1 (Figure 2). Since we focus on the spatial distribution of these variables (within and between cities), not their absolute magnitudes, we are confident about our results.

## 2.7. Decile Neighborhoods of Urban Surface Temperature

To estimate the gradient of mean $T_s$ within urban clusters during the study period, we first calculate the 10th–100th percentile of $T_s$ within each cluster using Moderate Resolution Imaging Spectroradiometer (MODIS) observations (MYD11A1.006 and MOD11A1.006) (Wan, 2006). These percentile values are from the mean pixel-level information (by averaging available daily satellite scenes) for July 2019. Different percentile values are obtained for the four cases, namely Terra daytime overpass ($\approx$10:30 a.m. local time), Aqua daytime overpass ($\approx$1:30 p.m. local time), Terra nighttime overpass ($\approx$10:30 p.m. local time), and Aqua nighttime overpass ($\approx$1:30 a.m. local time). Of these, we focus mostly on the daytime values, particularly for the Aqua overpass, which is close to the time of maximum $T_a$ and $HI_0$ (Figure S1 in Supporting Information S1). Using these percentile values as boundary conditions, we separate each urban cluster into 10 decile neighborhoods with each neighborhood representing a decile of $T_s$ variation. In other words, pixels with July mean $T_s$ values between >0th and 10th percentile of all mean $T_s$ values in a cluster are put into the $10^{th}$ percentile neighborhood (or first decile neighborhood), and so on till the 100th percentile neighborhood or 10th decile neighborhood, which includes mean $T_s$ values between >90th and 100th percentile. The decile neighborhoods are different for Terra and Aqua as well as for days and nights. An example of these decile neighborhoods is shown for Madrid, Spain in Figure 1b. Note that, for this particular cluster, the $T_s$ gradient does not increase as we reach the city center. This is intended since our goal is to examine whether the decile neighborhoods, as determined by satellite observations, are a reasonable proxy for the $T_a$ and $HI_0$ gradients.

After the decile neighborhoods are generated, each Netatmo station is grouped into a neighborhood for the four cases corresponding to the satellite overpass times. All these geospatial analyses are done on the Google Earth Engine cloud computing platform (Gorelick et al., 2017).

## 2.8. Matching CWS Data With Satellite-Derived Estimates

We extract the daily $T_s$ and exact MODIS viewing time for each $\approx$1 km pixel corresponding to the Netatmo stations that are either in a $T_s$ decile neighborhood or in the rural background. The satellite viewing time is then converted from local time to coordinated universal time based on the recommendations in the MODIS user guide

(Wan, 2006) of subtracting (in hours) the quotient when dividing the longitude of the pixel (in this case, the CWS location) by 15° and then adjusting by the daily hour bounds (>24 hr or <0 hr). The Netatmo observations are then matched with the daily MODIS $T_s$ when the Netatmo observation time is within 30 min of the MODIS viewing time.

Similar to $T_s$, we also extract the Normalized Difference Vegetation Index (NDVI), a satellite-derived proxy for live green vegetation (Rouse et al., 1974), from MODIS observations. This index takes advantage of the fact that plants absorb light in the red (RED) bands and reflect near-infrared (NIR) radiation, since NIR cannot be used in photosynthesis, and is given by

$$NDVI = \frac{NIR - RED}{NIR + RED} \tag{11}$$

The NDVI values are derived from 16-day composites corresponding to each Netatmo station and daytime overpass (MYD13A2 and MOD13A2 for Aqua and Terra, respectively) and joined with all observations at that station. The monthly means of NDVI for July 2019 are used for the final analysis since daily variability is not as relevant for NDVI and urban surface vegetation would remain relatively unchanged within a single month. In all cases, only clear-sky pixel values are used for analysis and satellite observations for the days with missing Netatmo observations (both $T_a$ and RH) due to quality-screening are also removed.

We also calculate monthly precipitation rate corresponding to each cluster from the monthly composites generated from the passive-microwave observations from the Global Precipitation Measurement mission (NASA Goddard Earth Sciences Data and Information Services Center, 2019). This analysis is done to examine how urban-rural differences in the variables of interest (see below) vary with the moisture availability of the background climate.

## 2.9. Urban-Rural Differences

Netatmo stations within the urban clusters and their corresponding satellite-derived values are used to estimate the urban $T_a$ ($T_{a,u}$), RH ($RH_u$), $HI_0$ ($HI_{0,u}$), $T_s$ ($T_{s,u}$), and NDVI ($NDVI_u$). The corresponding rural variables, $T_{a,r}$, $RH_r$, $HI_{0,r}$, $T_{s,r}$, and $NDVI_r$ are from the stations in the background reference areas. Only those cases were considered for which there were at least 10 stations in both the urban clusters and their surrounding references. This leaves 557 (603) urban clusters with 40,560 (42,745) unique stations for Aqua (Terra) daytime overpass. The urban-rural differences are thus:

$$\Delta T_a = T_{a,u} - T_{a,r} \tag{12}$$

$$\Delta RH = RH_u - RH_r \tag{13}$$

$$\Delta HI_0 = HI_{0,u} - HI_{0,r} \tag{14}$$

$$\Delta T_s = T_{s,u} - T_{s,r} \tag{15}$$

$$\Delta NDVI = NDVI_u - NDVI_r \tag{16}$$

Of these, $\Delta T_a$ is equivalent to the commonly studied CUHI and $\Delta T_s$ is similar to SUHI (Bonafoni et al., 2015; Chakraborty et al., 2017; Du et al., 2021; Venter et al., 2021). Although RH is a function of both absolute moisture content and ambient temperature, we call its urban-rural differences the UDI effect since it is a standard weather-relevant variable and one of the inputs used to estimate $HI_0$ (Equation 1). There is currently lack of consensus on a standard metric for urban moisture content, though it is commonly accepted that urban areas are drier due to removal of vegetation and pervious surfaces (Wang et al., 2021). For comparison, we also calculate the difference in absolute humidity (AH) between urban areas and their background references by combining the Netatmo observations with surface pressure estimates from ERA5-Land (Muñoz-Sabater et al., 2021). During the Aqua daytime overpass, roughly 54.3% of the urban clusters show lower AH than their background references with a mean $\Delta AH$ of $-8.7 \times 10^{-5}$ kg m$^{-3}$, confirming the presence of UDIs using both RH and AH. Similar urban-rural differences are also calculated for the humidex and the other heat indices. The use of the MODIS pixels overlaying the Netatmo locations to calculate $\Delta T_s$ leads to reasonable apples-to-apples comparison. The use of this approach might explain why the correlation coefficient between $\Delta T_s$ and $\Delta T_a$ here (Figure 7a) is

slightly higher than that in a previous study (Venter et al., 2021), which compared the Netatmo-derived $\Delta T_a$ with urban cluster mean $\Delta T_s$.

### 2.10. Intra-Urban Gradients

Although the analysis above is done for co-located pixels, the threshold for the minimum number of stations used (10) is insufficient to represent the mean climatic state of the clusters. Moreover, it is important to also analyze how well $T_s$, which has been extensively used as a proxy for the intra-urban variability in urban temperatures (Benz & Burney, 2021; Chakraborty et al., 2019, 2020; Hoffman et al., 2020; Hsu et al., 2021; Hulley et al., 2019), represents the within-city variability in $HI_0$. To address this, we estimate the intra-urban gradients in $T_s$, $T_a$, RH, and $HI_0$. The intra-urban gradient in station-level $T_s$ is calculated by first choosing those clusters with at least 10 stations in every decile neighborhood as well as the rural background, and then averaging the daily pixel-level MODIS $T_s$ in July 2019 that also had CWS measurements of $T_a$ and RH for each region. This analysis allows us to check how well the Netatmo observations capture the overall spatial variability in $T_s$, as represented by the decile neighborhoods, using the corresponding $T_s$ pixels overlaying those stations. The average value of the satellite-derived $T_s$ for the pixels overlaying the Netatmo stations increase for increasing decile neighborhoods in all clusters (Figure 2, Figure S4 in Supporting Information S1). Similarly, the gradients corresponding to these regions for $T_a$, RH, and thus $HI_0$ are computed from the corresponding hourly Netatmo measurements. Figure 1c shows the total number of observations as well as the number of unique Netatmo stations considered when calculating these intra-urban gradients corresponding to the Terra and Aqua daytime overpass. Overall, we use 153 and 155 clusters to generate intra-urban gradients corresponding to Aqua and Terra daytime overpass, respectively.

### 2.11. Statistical Analysis

To check whether the distributions of the chosen variables ($T_s$, $T_a$, RH, $HI_0$, humidex, $HI_1$, $HI_2$, $HI_3$, and $HI_4$) are statistically different between regions (either between urban clusters and their rural backgrounds or between the rural backgrounds and the decile neighborhoods), we use the Mann-Whitney two-sample test (Wilcoxon et al., 1992). This nonparametric test allows us to check if two samples come from the same population, with lower $p$-values supporting the rejection of the null hypothesis that both the distributions are same. We choose a significant level of 0.01 to reject the null hypothesis, but also specify when the $p$-value is below 0.001 and 0.0001 in the summary tables (Tables S1–S4 in Supporting Information S1).

In addition to simple linear regressions between pairs of variables to test for their correlation and sensitivity, we also separate the control of $T_a$ and RH on the intra-urban gradient of $HI_0$ within clusters by representing $HI_0$ as a linear combination of $T_a$ and RH:

$$HI_0 = \alpha_1 T_a + \alpha_2 RH \tag{17}$$

where $\alpha_1$ and $\alpha_2$ are the sensitivities of $HI_0$ to $T_a$ and RH, respectively, as determined using multiple linear regressions for each urban cluster (Figure 3a). Since $T_a$ and RH have widely different range of values, we also consider a standardized form of this representation, given by:

$$HI_0 = \alpha_{1,std} \frac{T_a}{T_{a,r}} + \alpha_{2,std} \frac{RH}{RH_r} \tag{18}$$

where $T_{a,r}$ and $RH_r$ are the corresponding mean values for the rural backgrounds and the standardized sensitivities are $\alpha_{1,std}$ and $\alpha_{2,std}$ (Figure 3b). A similar linear model is also used to express $\Delta HI_0$ as a function of $\Delta T_a$ and $\Delta RH$.

## 3. Results

### 3.1. Urban-Rural Differences in Temperature, Humidity, and Heat Stress

Across 557 urban clusters in Europe (Figure 1a), the mean $\Delta T_s$ (urban minus rural $T_s$) corresponding to the Aqua satellite's daytime overpass ($\approx$1:30 p.m. local time) was 2.06°C (5$^{th}$ percentile = −1.3°C; 95th percentile = 5.25°C) based on satellite observations over 40,560 unique CWSs with data availability after quality screening (Figure 4a). At $\approx$10:30 a.m. local time, corresponding to the Terra satellite's daytime overpass, the mean $\Delta T_s$ over 603 clusters was slightly lower at 1.68°C (5th percentile = −1.22°C; 95th percentile = 4.48°C;
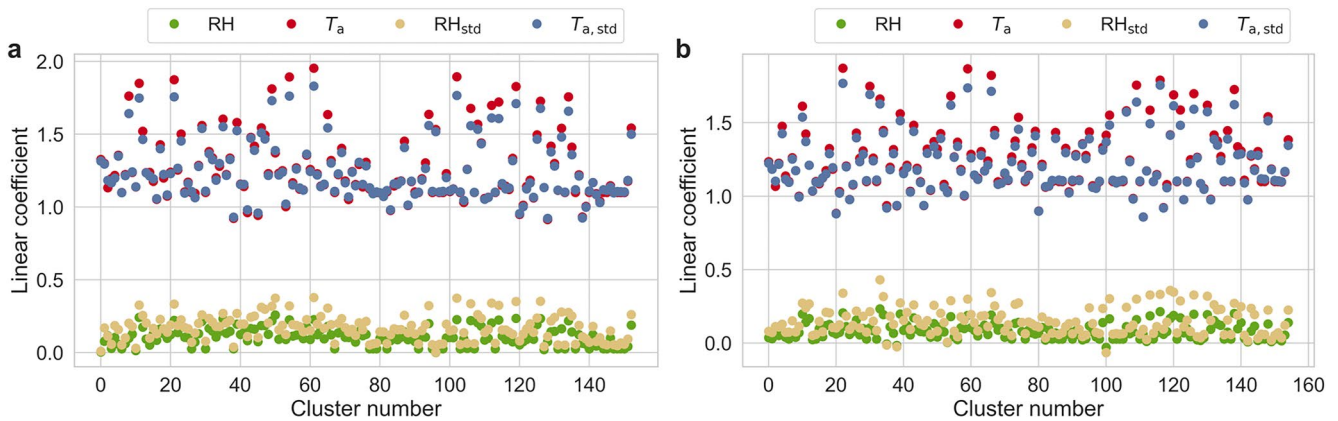
**Figure 3.** Control of air temperature and relative humidity on heat stress. Values of coefficients of multi-linear regressions (of the form $HI_0 = \alpha_1 T_a + \alpha_2 RH$) for all urban clusters in Europe that have sufficient data for (a) Aqua and (b) Terra overpass times, respectively. The $std$ values correspond to similar multi-linear regressions, but with standardized variables (i.e., $HI_0 = \alpha_{1,std} T_a/T_{a,r} + \alpha_{2,st} dRH/RFr$) where $r$ variables are for the rural background.

Figure S2a in Supporting Information S1). In contrast, the mean urban-rural difference in $T_a$ ($\Delta T_a$) from the CWS measurements was only 0.12°C (5th percentile = −1.92°C; 95th percentile = 2.19°C) at ≈1:30 p.m. (Figure 4b) and 0.05°C (5th percentile = −2.18°C; 95th percentile = 2.17°C) at ≈10:30 a.m. (Figure S2b in Supporting Information S1). The lower $\Delta T_a$ than $\Delta T_s$ during daytime is consistent with previous results from various data sources and at multiple scales (Chakraborty et al., 2017; Du et al., 2021; Ho et al., 2016; Hoffman et al., 2020;
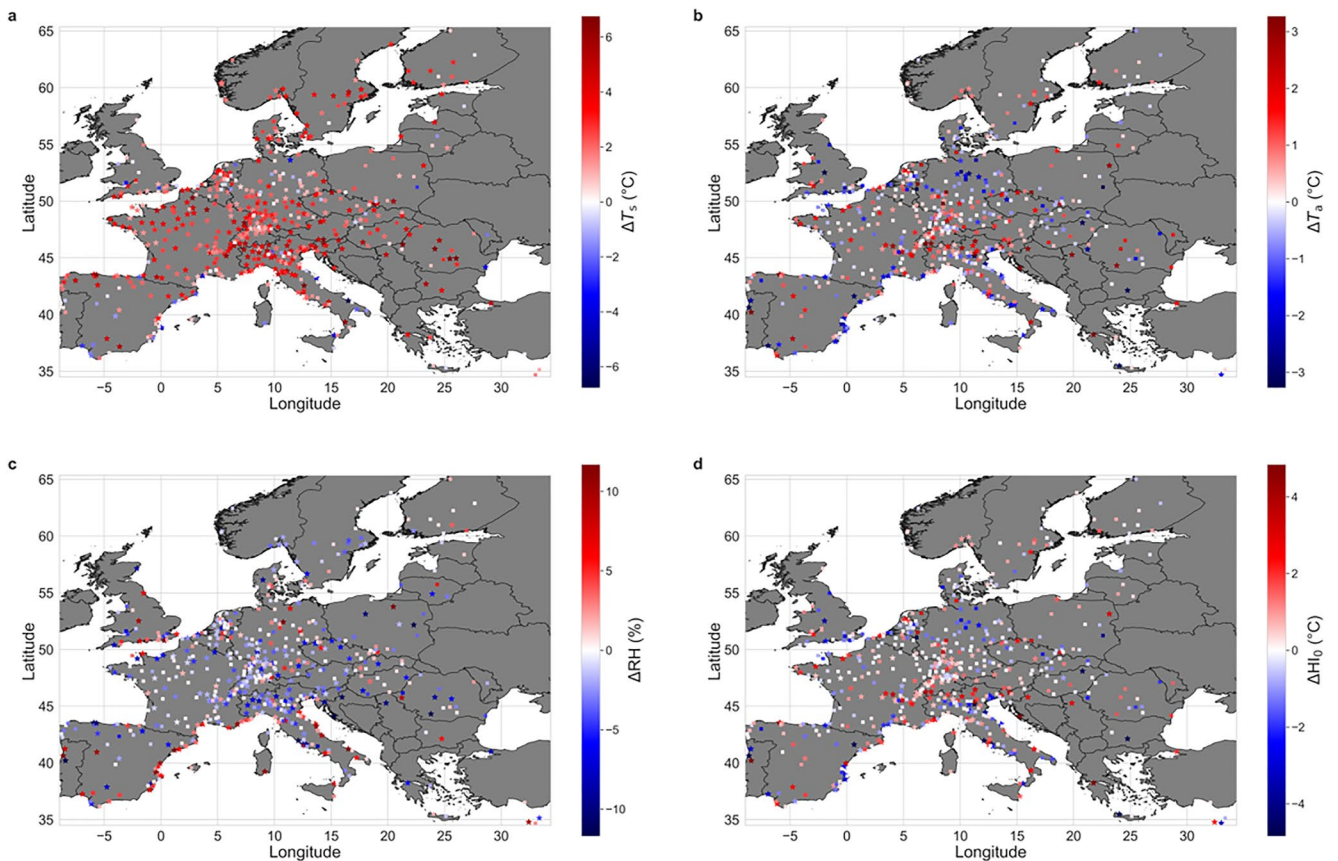


**Figure 4.** Urban-rural differences for Aqua day across urban clusters. Spatial distribution of urban-rural differences in (a) surface temperature ($\Delta T_s$), (b) air temperature ($\Delta T_a$), (c) relative humidity ($\Delta RH$), and (d) heat index ($\Delta HI_0$) for urban clusters in Europe at ≈1:30 p.m. local time. The stars represent clusters with statistically significant ($p < 0.01$) differences between urban and rural values.

Venter et al., 2021; Zhang et al., 2014). Urban areas are also generally drier than their surroundings with a mean urban-rural difference in RH ($\Delta$RH) of $-0.6\%$ (5th percentile $= -7.16\%$; 95th percentile $= 6.43\%$) for the Aqua daytime overpass (Figure 4c). The mean $HI_0$ at urban CWSs is slightly higher than that for rural CWSs (mean urban-rural difference in $HI_0$ ($\Delta HI_0$) $= 0.08°C$; 5th percentile $= -2.28°C$; 95th percentile $= 2.58°C$; Figure 4d).

Evidently, due to biophysical and morphological differences in urban and rural characteristics (L. Zhao et al., 2014; Qian et al., 2022), as well as uncertainties and lack of statistical representativeness of the measurements, there are large variabilities. However, the larger scale patterns are consistent, with 87.6% (488) of the clusters showing positive $\Delta T_s$ (with 73.1% showing statistically significant differences from zero at the significance level of 0.01), which goes down to 55.1% for positive $\Delta T_a$ (37% with statistically significant differences) and 54.8% for positive $\Delta HI_0$ (31.8% with statistically significant differences) for the Aqua daytime overpass. Similar patterns are seen corresponding to the Terra daytime overpass (Figure S2 in Supporting Information S1). In both cases, urban areas are generally drier than their surroundings or $\Delta$RH is negative (59.8% of clusters at $\approx$1:30 p.m. and 58.8% at $\approx$10:30 a.m.; also seen when using AH instead of RH), which would reduce $HI_0$, all else remaining constant. We find $\Delta T_a$ to be over 11 times more important for modulating $\Delta HI_0$ than $\Delta$RH (slope coefficients of 1.37 and 0.12 for $\Delta T_a$ and $\Delta$RH, respectively, from a multiple linear regression). Although the compensating effects of $T_a$ and RH on $HI_0$ makes conceptual sense, what is surprising is that the urban-rural differences in $HI_0$ is so close to zero for cities during a heatwave period, with less than a third showing statistically significant differences between the urban area and its rural reference. These results weaken a common premise in many previous studies where increased urban $T_s$ is expected to indicate adverse urban impact on overall heat vulnerability (Hsu et al., 2021; L. Zhao et al., 2017; Manoli et al., 2019; Mentaschi et al., 2022).

Consistent with previous observational and modeling estimates (Chakraborty & Lee, 2019; L. Zhao et al., 2014; Manoli et al., 2019), $\Delta T_s$ is higher for wetter climate and lower for drier areas, as seen when binned by quartiles of precipitation rate or accumulated precipitation for the same period (Figures S3a and S3e in Supporting Information S1). However, this relationship with background climate weakens for $\Delta T_a$ (Figures S3b and S3f in Supporting Information S1) and almost disappears for $\Delta HI_0$ (Figures S3d and S3h in Supporting Information S1), evidently due to thermodynamic moisture feedback through $\Delta$RH (Figures S3c and S3g in Supporting Information S1). As such, generalized mitigation strategies derived from information about background climate (Manoli et al., 2019) may reduce $\Delta T_s$ but would have a much smaller impact on $\Delta HI_0$.

## 3.2. Spatial Gradients in the Urban Thermal Environment

Several studies (Benz & Burney, 2021; Chakraborty et al., 2019; Hsu et al., 2021; Hulley et al., 2019; Maimaitiyiming et al., 2014) have examined intra-urban variability in temperature using satellite-derived $T_s$. To test whether $T_s$ is a useful proxy for urban $HI_0$ variability within cities, we calculate the intra-urban gradients in $T_s$, $T_a$, RH, and $HI_0$ using those clusters (153 for Aqua and 155 for Terra) with enough (>10) CWSs in each decile neighborhood and the rural background (see Section 2; Figure 5). During the Aqua daytime overpass, the gradient of $T_a$ along the decile neighborhoods is weaker than that for $T_s$ with 121 of the 153 clusters showing a positive slope, which goes down to 114 for $HI_0$. Higher $T_s$ decile neighborhoods are generally drier, with RH showing a negative slope with increasing $T_s$ in 83.6% (128) of the clusters (Figure 6a). Overall, the relationship between $T_s$ and $T_a$, although positive (mean correlation coefficient $r = 0.34$), shows a sensitivity (given by the slope of the linear regressions) much lower than 1 (mean slope $= 0.12$; Figure 6a). This sensitivity decreases further for $HI_0$ (0.09) due to the compensating effects of decreasing RH and increasing $T_a$ on $HI_0$ (Figure 6b). The standardized $T_a$ rises at roughly half the rate of the decrease in standardized RH within cities with the linear sensitivity of $HI_0$ to $T_a$ being around seven times the sensitivity to RH (Figure 3). Consequently, the urban $HI_0$ in only two of the decile neighborhoods show statistically significant differences ($p < 0.01$) from the $HI_0$ in the rural background (Table S1 in Supporting Information S1). In contrast, 9, 7, and 3 of these 10 neighborhoods show statistically significant differences from the background climate for $T_s$, RH, and $T_a$, respectively. Similar results are seen for other heat indices (Tables S1 and S2 in Supporting Information S1) and corresponding to the Terra daytime overpass (Figure S4 in Supporting Information S1) with 9, 2, 7, and 0 of these 10 neighborhoods showing statistically significant differences from the background climate for $T_s$, $T_a$, RH, and $HI_0$, respectively.
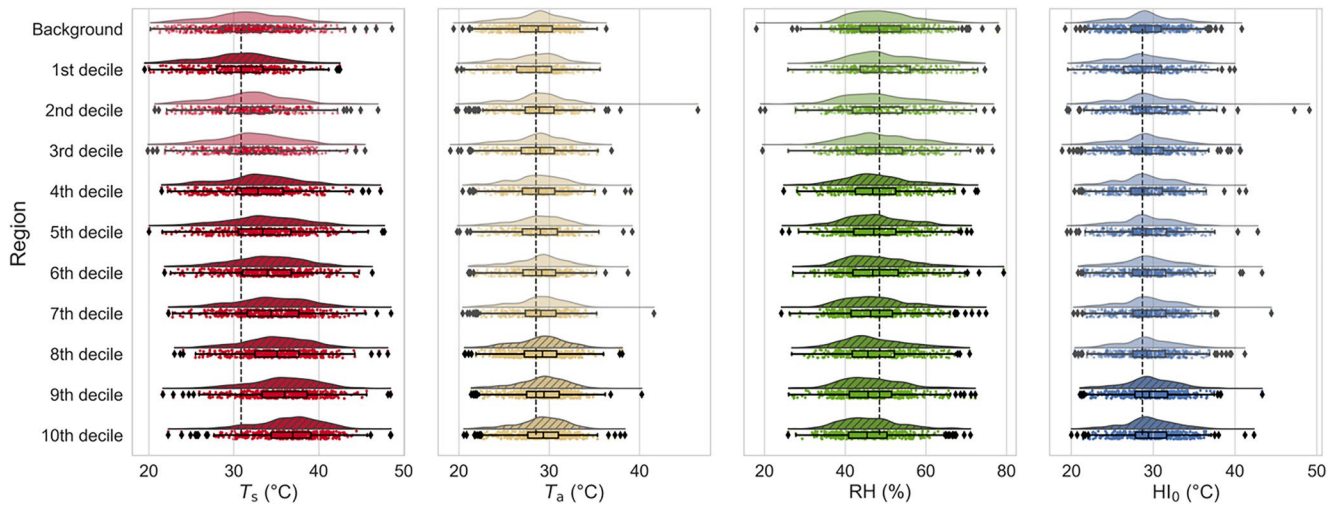
**Figure 5.** Intra-urban gradients of variables. Distributions of composite mean surface temperature ($T_s$), air temperature ($T_a$), relative humidity (RH), and heat index ($HI_0$) in each of the $T_s$ decile neighborhoods across the urban clusters considered. The vertical dashed lines mark the median of the distribution of the corresponding variable in the 1st $T_s$ decile neighborhood. Decile neighborhoods that show statistically significant ($p < 0.01$) differences from the background reference values are shown using hatched density plots and darker shades. All calculations are for ≈1:30 p.m. local time.

### 3.3. Role of Urban Vegetation

There is strong evidence that urban vegetation reduces $T_s$ (Chakraborty & Lee, 2019; Chakraborty et al., 2020; Paschalis et al., 2021; Schwaab et al., 2021), which is captured in our analysis. In 150 of the 153 clusters, the NDVI, a satellite-derived proxy for vegetation cover and vigor, is inversely correlated with $T_s$ (Figure 6c). However, NDVI has weaker associations with $T_a$ (mean $r = -0.81$ for $T_s$; $-0.26$ for $T_a$) with $T_a$ also showing a lower sensitivity to NDVI (mean slope = $-3.01$°C per unit NDVI) than $T_s$ ($-26.76$°C per unit NDVI). That vegetation has a weaker control on local-scale $T_a$ than $T_s$ is consistent with field-level observations (Novick & Katul, 2020). The association with NDVI weakens further for $HI_0$, with roughly 30.7% of clusters showing a positive correlation with a weak mean sensitivity of around $-2.15$°C per unit NDVI. Similar results are seen at ≈10:30 a.m. with 97.4% (151), 67.7% (105), and 63.2% (98) of the clusters, showing a negative association with NDVI in the decile neighborhoods for $T_s$, $T_a$, and $HI_0$, respectively (Figure S5c in Supporting Information S1). The mean sensitivities to NDVI at ≈10:30 a.m. range between $-22.71$°C for $T_s$ and $-2.81$°C for $HI_0$. Similarly, the intra-urban variability in $\Delta HI_0$ is weakly associated with $\Delta NDVI$ for both the Aqua and Terra daytime overpasses (coefficient of determination $r^2 \leq 0.02$; Figure 7h, Figure S6h in Supporting Information S1) compared to $\Delta T_s$ ($r^2 \approx 0.30$; Figure 7e, Figure S6e in Supporting Information S1). The associations between $\Delta HI_0$ and $\Delta NDVI$ are similarly weak at night (Figure S7 in Supporting Information S1). We stress that the assumed linear associations between these variables is to provide easier interpretability through the slope coefficients. Though the true relationships can be nonlinear (for instance, RH and $T_a$ impact $HI_0$ nonlinearly; see Figure 8), the overall stronger associations for $T_s$ compared to $T_a$ and $HI_0$ should remain.

## 4. Discussion

### 4.1. Deficiencies in Surface Temperature for Studying Urban Areas

Satellite-derived $T_s$ is widely used for urban research (Bechtel et al., 2019; Benz & Burney, 2021; Chakraborty & Lee, 2019; Clinton & Gong, 2013; Manoli et al., 2019; Paschalis et al., 2021; Zhou et al., 2018). For observational studies, this is due to the availability of global and spatially continuous satellite measurements, which enable, among other things, analyses of intra-urban and inter-urban variability; difficult using ground-based measurements. Satellite-derived $T_s$ is also used to develop and evaluate models (L. Zhao et al., 2014; Manoli et al., 2019). Conceptual models of $T_s$ are easier to formulate than those for $T_a$ or $HI_0$, due to strong coupling between $T_s$ and the surface energy budget (Li et al., 2019; L. Zhao et al., 2014). Although $T_s$ and $T_a$ are not strongly correlated over urban areas, especially relevant for public health (Ho et al., 2016; Stone et al., 2019), studies have assumed, either implicitly or explicitly, that $\Delta T_s$ can still be useful for making decisions about urban heat mitigation (Benz
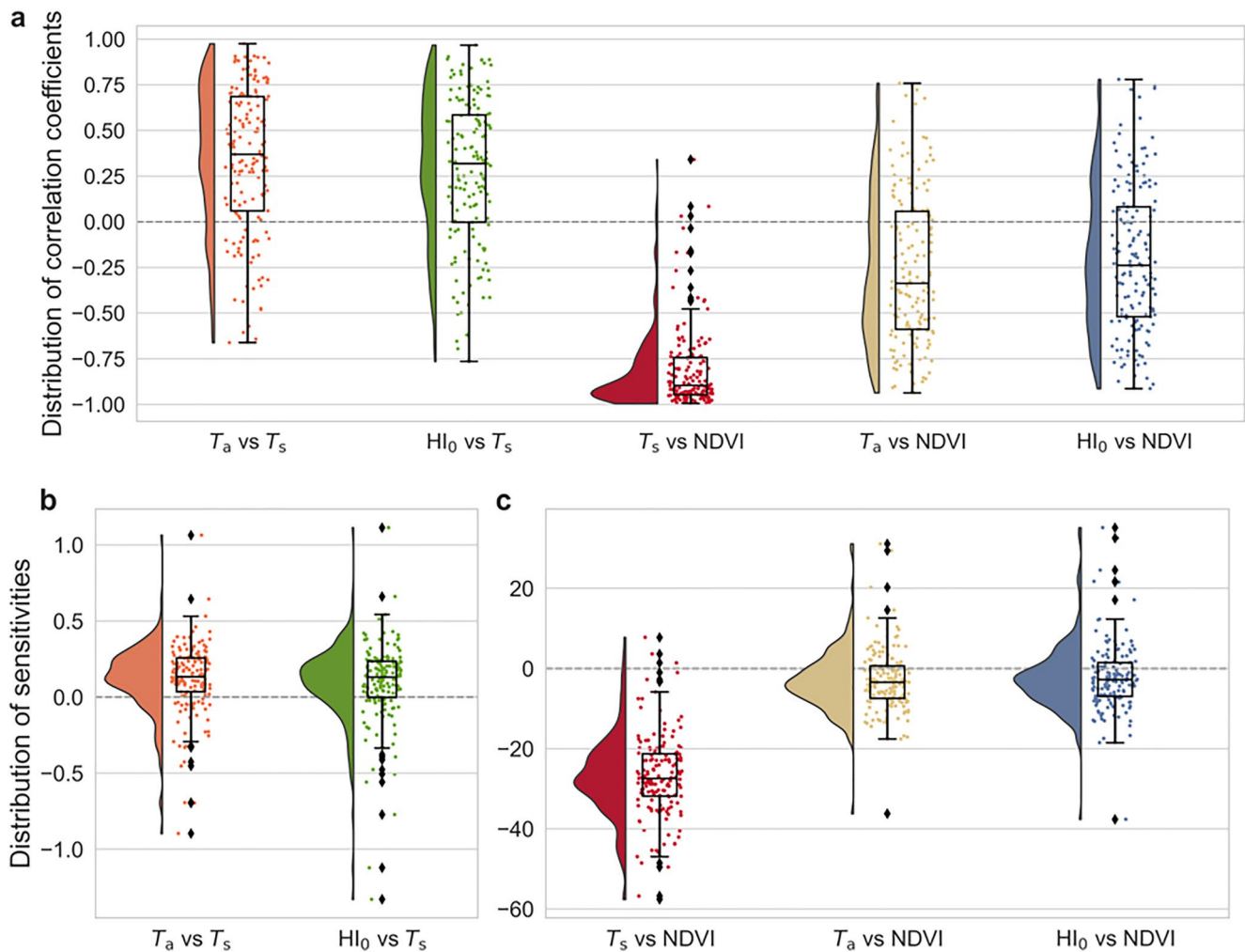
**Figure 6.** Associations between variables within urban clusters. Panel (a) shows the distributions of the correlation coefficient ($r$) of linear regressions between surface temperature ($T_s$) and air temperature ($T_a$), $T_s$ and heat index ($HI_0$), Normalized Difference Vegetation Index (NDVI) and $T_s$, NDVI and $T_a$, and NDVI and $HI_0$, respectively, for urban clusters in Europe. Each data point is from a linear regression between pairs of variables for a cluster. The linear regressions have a sample size of ten (one for each $T_s$ decile neighborhood). Panels (b and c) show the distributions of the slope of those linear regressions, or the sensitivity of one variable to unit changes in the other. The unit of sensitivity in panel (c) is °C per unit NDVI. All calculations are for ≈1:30 p.m. local time.

& Burney, 2021; Chakraborty et al., 2020; Hsu et al., 2021; Hulley et al., 2019; L. Zhao et al., 2014; Manoli et al., 2019). We find that for cities in Europe during a heatwave period, the correlations between urban-scale $\Delta T_s$ and $\Delta T_a$ are fairly weak, particularly during daytime ($r^2 = 0.10$ for Aqua; 0.09 for Terra; Figure 4a, Figure S6a in Supporting Information S1) with only 21% of the variability in $\Delta T_s$ (slope = 0.21) among cities expected for $\Delta T_a$.

Furthermore, our analysis shows that the inter-urban variability in $\Delta HI_0$ is weaker still when correlated with that of satellite-derived $\Delta T_s$ ($r^2 = 0.04$; Figure 7c, Figure S6c in Supporting Information S1), making $T_s$ a poor proxy for the urban impact on outdoor heat vulnerability. As such, any insights gained using $T_s$, whether using observations or models, may not be strongly relevant for mitigating urbanization-induced heat stress. Note that we examine urban-rural differences to isolate the urban influence on these variables, rather than absolute $HI_0$, which would regulate total heat-related hazard in cities (Martilli et al., 2020). This is done to account for differences in absolute $HI_0$ in cities due to background climate.

Coarse to medium-resolution $T_s$ from satellites have been used for hotspot analysis within cities (Hulley et al., 2019; Maimaitiyiming et al., 2014; Mentaschi et al., 2022). Several studies have taken advantage of the spatial continuity of satellite observations to map intra-urban variability of $T_s$ across cities with implications for environmental disparities (Benz & Burney, 2021; Chakraborty et al., 2019; Hsu et al., 2021). We find that for
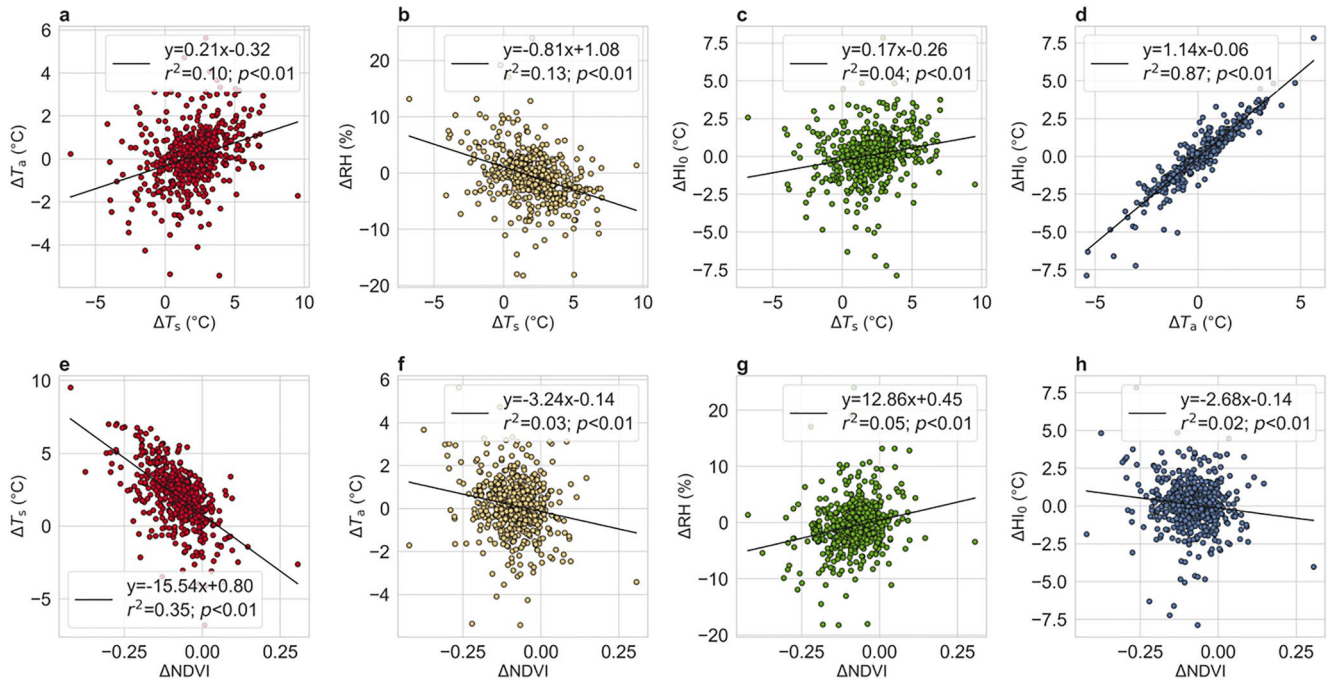
**Figure 7.** Associations between variables across urban clusters. Associations between urban-rural differences in (a) surface temperature ($\Delta T_s$) and air temperature ($\Delta T_a$), (b) $\Delta T_s$ and relative humidity ($\Delta$RH), (c) $\Delta T_s$ and heat index ($\Delta$HI$_0$), (d) $\Delta T_a$ and $\Delta$HI$_0$, (e) Normalized Difference Vegetation Index ($\Delta$NDVI) and $\Delta T_s$, (f) $\Delta$NDVI and $\Delta T_a$, (g) $\Delta$NDVI and $\Delta$RH, and (h) $\Delta$NDVI and $\Delta$HI$_0$ across urban clusters in Europe. Each dot represents one cluster, and the lines and equations of best fit are shown. All calculations are for $\approx$1:30 p.m. local time.
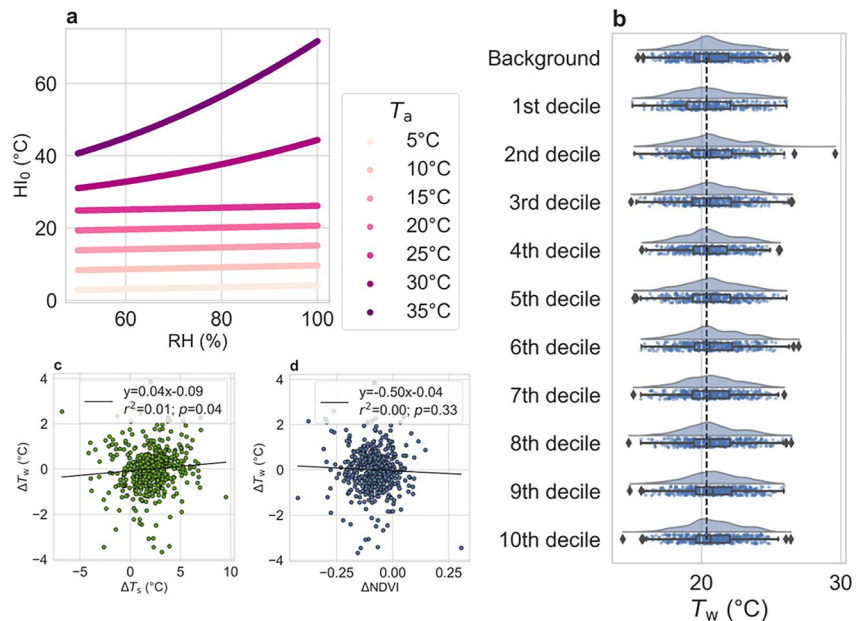


**Figure 8.** Humidity and metrics of heat stress. Panel (a) shows the dependence of the heat index (HI$_0$) used by the US National Weather Service on relative humidity (RH) for different values of air temperature ($T_a$). Panel (b) shows distributions of composite mean surface wet-bulb temperature ($T_w$) in each of the $T_s$ decile neighborhoods across the urban clusters considered (similar to Figure 5). Panels (c and d) show associations between urban-rural differences in surface temperature ($\Delta T_s$) and $T_w$ ($\Delta T_w$), and Normalized Difference Vegetation Index ($\Delta$NDVI) and $\Delta T_w$, respectively, across urban clusters in Europe. Each dot represents one cluster and the lines and equations of best fit are shown. All calculations in panels (b–d) are for $\approx$1:30 p.m. local time.

the cities considered here, $T_s$ is a poor proxy for the intra-urban variability in $HI_0$ or other heat indices (including humidex, used in heat warning systems). Even the 95th and 98th percentiles of hourly $HI_0$ ($HI_{0,95}$ and $HI_{0,98}$, respectively) do not show statistically significant differences from the background in most of the decile neighborhoods (Figure S8 and Table S3 in Supporting Information S1). Future multi-city studies should focus on covariance of more physiologically relevant heat exposure metrics with socioeconomic variables to re-evaluate the magnitude of these environmental disparities, if any.

This is not to say that examining $T_s$ over cities is pointless. Nighttime $\Delta HI_0$ ($\approx$1:30 a.m. local time) is generally positive (Figure S9 in Supporting Information S1), and moderately correlated with $\Delta T_s$ ($r^2 = 0.21$; $p < 0.01$) across (Figure S7c in Supporting Information S1) and within cities (Table S4 in Supporting Information S1), which might explain why previous studies have shown associations between nighttime $T_s$ and heat-related mortality (Laaidi et al., 2012; Murage et al., 2017). Moreover, high $T_s$ does increase radiant heat exposure and is the lower boundary for the atmospheric column, which consequently modulates the surface energy budget and local weather (Arnfield, 2003). Ultimately, more accurate estimates of all-condition heat stress within cities requires more ground-level observations, not just of standard meteorological variables, but also exposure to radiation and wind speed, which are not available from these CWSs. Moreover, CWS sensors are not research-grade and frequently influenced by less-than-ideal placement, insufficient site metadata, and usually lack radiation shields, though that last issue has minimal impact since we primarily deal with distributions, not absolute values (Figure 2).

Urban climate research has generally encouraged urban tree planting due to their local evaporative cooling potential (Chakraborty & Lee, 2019; Chakraborty, Biswas, et al., 2022; Li et al., 2019; Paschalis et al., 2021; Schwaab et al., 2021; Wong et al., 2021; Ziter et al., 2019). However, reductions in $T_s$ through evaporation, which is the primary focus of most of these studies, do not imply equivalent reductions in $T_a$ (Novick & Katul, 2020). This is further complicated when we consider $HI_0$ due to the local-scale increase in RH due to vegetation (Krayenhoff et al., 2021; Meili et al., 2020). We find that the efficiency of reducing $HI_0$ within cities using urban vegetation is weakened ($-2.15°C$ for a hypothetical unit change in NDVI, spanning half the physically possible range), as seen from the linear correlations, due to the competing effects of reduced $T_a$ and enhanced RH. Moreover, the urban-rural differences in vegetation are not associated with the urban-rural differences in $HI_0$ across cities due to these same competing effects (Figures 7f and 7g, Figures S6f and S6g in Supporting Information S1). However, note that shading effect of trees is also important and reduces the radiant heat exposure on pedestrians at the micro scale, although urban form can also serve this purpose (Middel et al., 2021; Q. Zhao et al., 2018). Moreover, there are several co-benefits of urban vegetation, from increased carbon sequestration to reduced air pollution to multiple beneficial health outcomes, beyond any reduction in local temperature (Chakraborty, Biswas, et al., 2022; Fargione et al., 2018; Fong et al., 2018; Remme et al., 2021). Overall, mitigation strategies that rely on urban vegetation should carefully consider the realistic efficiency of street trees to improve thermal comfort at multiple scales (vs. competing strategies) in addition to those other co-benefits for accurate cost-benefit analyses. Besides, when the reduction in satellite-derived $T_s$ due to surface vegetation is usually examined (Chakraborty, Biswas, et al., 2022; Paschalis et al., 2021; Schwaab et al., 2021; Wong et al., 2021), what is compared is the association of $T_s$ of the top of the canopy (what the satellite "sees") with some measure of vegetation. Since this is not physically equivalent to what a pedestrian would feel either underneath the tree canopy or near it, we need to be cautious about quantitative estimates of the cooling potential of urban vegetation derived from satellite measurements of $T_s$. Similarly, models used to examine urban heat stress or urban heat mitigation must incorporate accurate urban vegetation to represent realistic cities, which is currently missing, simplistic, or still under development (Krayenhoff et al., 2020, 2021; L. Zhao et al., 2017, 2021; Meili et al., 2020).

## 4.2. Relative Importance of Humidity for Heat Stress

The role of humidity in human physiological response to heat is recognized (Anderson et al., 2013; Ebi et al., 2021; Vargas et al., 2020). How important humidity is relative to $T_a$ for heat stress is however still an open question (Anderson et al., 2013; Sherwood, 2018; Vargas et al., 2020). For Europe, we find $T_a$ to be around seven times more important than RH for capturing both the inter-urban and intra-urban variability in $HI_0$ (Figure 3). However, $HI_0$ is known to have a low sensitivity to RH compared to many other heat indices (Sherwood, 2018). Moreover, most parts of Europe, even at their warmest, would have a further lower sensitivity of $HI_0$ to RH due to the $HI_0$ formulation (Equations 1 and 2; Figure 8a). This is particularly apparent at night, when $T_a$ and $HI_0$

are found to be strongly coupled (Figure S7d in Supporting Information S1) since it uses the simple linear equation (Equation 1) with much higher importance given to $T_a$ than RH. Since the impact of RH on $HI_0$ increases nonlinearly with increasing $T_a$ (Figure 8a), in warmer and more humid regions, such as in the tropics, the RH reduction due to urbanization could have more noticeable effect on moderating urbanization-induced heat stress (Mishra et al., 2020). Besides, the similar magnitudes of changes in $T_a$ and $HI_0$, say when correlated with NDVI (Figures 6c, 7f and 7h), can be misleading without contextualizing that unit changes in $HI_0$ are not physiologically equivalent to a unit change $T_a$. For instance, changing $T_a$ from 5 to 35°C leads to changes in $HI_0$ from 5°C to over 70°C (Figure 8a). Ideally, these variables should be compared in the context of public health, though heat-related health-outcome data are generally not available at such (intra-urban) scales to accurately to do this.

Several recent climate-related studies have also used $T_w$ as a heat stress metric (L. Zhao et al., 2021; Mishra et al., 2020; Raymond et al., 2020). In contrast to the empirical measures of heat stress, $T_w$ has a clear thermodynamic basis, with values above 35°C inducing hyperthermia in humans and other mammals, and even lower values of $T_w$ potentially having mortality and morbidity impacts (Raymond et al., 2020; Sherwood & Huber, 2010). $T_w$ is more strongly controlled by humidity than $HI_0$ and is essentially a measure of the moisture content of an air parcel. This higher sensitivity of $T_w$ to RH can be illustrated by calculating $T_w$ and urban-rural differences in $T_w$ ($\Delta T_w$) using the CWS measurements. $\Delta T_w$ is slightly negative (−0.002°C) and shows even weaker (compared to those against $\Delta HI_0$; Figure 7) and statistically insignificant correlations with $\Delta T_s$ and $\Delta$NDVI (Figures 8c and 8d). Moreover, none of the decile regions show statistically significant differences in $T_w$ from the background (Figure 8b). As such, although the moderating effect of decreasing RH on heat stress is both conceptually and observationally apparent, in the absence of health outcome data, the magnitude of this effect would depend on the measure of moist heat stress used (Buzan & Huber, 2020). This moist heat stress should also ideally be calculated using concurrent estimates of $T_a$ and RH. However, sometimes due to data scarcity, daily maximum $T_a$ is combined with daily mean RH to estimate heat stress, especially for future heat stress projections (Coffel et al., 2017; Woetzel et al., 2020). Due to the opposite diurnal cycle of $T_a$ and RH (Figure S1 in Supporting Information S1), using mean RH will overestimate heat stress (particularly relevant for $T_w$ due to strong RH sensitivity, but also important for other heat indices). Finally, for the use of $T_w$ as a heat index, it should be kept in mind that only higher absolute values (usually above 31°C) have been physiologically linked to human health response and under very specific conditions (completely wet and unclothed; Sherwood, 2018).

### 4.3. Limitations and Implications

The results of the present study do not necessarily imply that urban areas have no additional potential for heat stress compared to their surroundings or that we should not target cities for heat mitigation. Urban areas tend to have positive nighttime $\Delta T_a$ and $\Delta HI_0$, which contributes to mortality and morbidity during heatwaves (Laaidi et al., 2012; Murage et al., 2017). Even during daytime, we find large variabilities in $\Delta HI_0$, and the positive $\Delta HI_0$ would disproportionately impact public health given the high population densities in cities. Moreover, a source of uncertainty with CWS data is that they have sampling biases, with most sensors set up in residential areas, not in commercial districts where it is usually hotter (based on $T_s$; Hulley et al., 2019). Thus, we may be systematically avoiding non-residential areas when using CWS data, where pedestrians may still be exposed to higher-than-expected heat stress. For accurate use of CWS in urban research, it is also critical to have better site metadata, including exact location (for instance, distance from walls and paved surfaces), potential exposure to the sun (whether it is placed under shade as suggested by the manufacturer or not), and other non-ideal working conditions. Better quality control paradigms are also needed. Current methods, such as the "Crowd-QC" package (Napoly et al., 2018), make statistical assumptions about the data set that may miss extreme events and filter out real urbanization-induced signals. Finally, the heat indices used in this study are incomplete estimates of heat stress and only valid under shaded conditions since they do not include radiation.

The caveats above do not undermine the observation that within cities, urbanization-induced lower RH partly compensates for the higher $T_a$ when it comes to heat stress under shaded conditions, and that the spatial variability in this heat stress is poorly captured by satellite observations for the corresponding overlaying pixels. Note that these results are derived from observations in cooler temperate climate, and cities in other parts of the world may show differences in the strength, or lack thereof, of associations between these variables. However, on a conceptual level, we speculate that we will get qualitatively similar results with $T_s$ showing stronger variability than $T_a$ and $HI_0$ across scales. However, more observations, particularly for cities in arid and humid regions, are necessary

to confirm this hypothesis and quantify the extent of decoupling between $T_s$ and heat stress. In summary, we find compelling observational evidence that relying on $T_s$ to generate large-scale insights into the magnitude of urban $HI_0$ and recommendations for urban heat mitigation may be inappropriate. On a positive note, this mediating effect of the urbanization-induced heating and drying suggest that less effort may be needed to reduce urban thermal discomfort compared to their surroundings, leading to relatively higher benefits of urban-scale mitigation strategies that focus on heat stress. It is often said that "You can't manage what you can't measure." Our present study suggests that we may be often measuring the wrong variable for quantifying and mitigating the heat-related public health consequences of urbanization. In spite of the logistic and methodological simplicity of implementing satellite-derived $T_s$, we need more in situ observations of $T_a$, RH, wind speed, solar radiation, etc. and/or better urban-resolving models to more accurately characterize the urban thermal environment and quantify the efficiency of heat stress mitigation strategies as we prepare for a warmer and more urban future.

## Conflict of Interest

The authors declare no conflicts of interest relevant to this study.

## Data Availability Statement

The data analyzed and presented here can be found at: https://github.com/TC25/Europe_CWS. They are also archived through Mendeley Data (Chakraborty, Venter, et al., 2022).

## References

Alduchov, O. A., & Eskridge, R. E. (1996). Improved Magnus form approximation of saturation vapor pressure. *Journal of Applied Meteorology and Climatology*, *35*(4), 601–609. https://doi.org/10.1175/1520-0450(1996)035⟨0601:IMFAOS⟩2.0.CO;2

Anderson, G. B., Bell, M. L., & Peng, R. D. (2013). Methods to calculate the heat index as an exposure metric in environmental health research. *Environmental Health Perspectives*, *121*(10), 1111–1119. https://doi.org/10.1289/ehp.1206273

Arnfield, A. J. (2003). Two decades of urban climate research: A review of turbulence, exchanges of energy and water, and the urban heat island. *International Journal of Climatology*, *23*(1), 1–26. https://doi.org/10.1002/joc.859

Bechtel, B., Demuzere, M., Mills, G., Zhan, W., Sismanidis, P., Small, C., & Voogt, J. (2019). SUHI analysis using local climate zones—A comparison of 50 cities. *Urban Climate*, *28*, 100451. https://doi.org/10.1016/j.uclim.2019.01.005

Benz, S. A., & Burney, J. A. (2021). Widespread race and class disparities in surface urban heat extremes across the United States. *Earth's Future*, *9*(7), e2021EF002016. https://doi.org/10.1029/2021EF002016

Bonafoni, S., Anniballe, R., & Pichierri, M. (2015). Comparison between surface and canopy layer urban heat island using MODIS data. In *2015 Joint Urban Remote Sensing Event (JURSE)* (pp. 1–4).

Buzan, J. R., & Huber, M. (2020). Moist heat stress on a hotter Earth. *Annual Review of Earth and Planetary Sciences*, *48*(1), 623–655. https://doi.org/10.1146/annurev-earth-053018-060100

Chakraborty, T., Biswas, T., Campbell, L. S., Franklin, B., Parker, S. S., & Tukman, M. (2022). Feasibility of afforestation as an equitable nature-based solution in urban areas. *Sustainable Cities and Society*, *81*, 103826. https://doi.org/10.1016/j.scs.2022.103826

Chakraborty, T., Hsu, A., Manya, D., & Sheriff, G. (2019). Disproportionately higher exposure to urban heat in lower-income neighborhoods: A multi-city perspective. *Environmental Research Letters*, *14*(10), 105003. https://doi.org/10.1088/1748-9326/ab3b99

Chakraborty, T., Hsu, A., Manya, D., & Sheriff, G. (2020). A spatially explicit surface urban heat island database for the United States: Characterization, uncertainties, and possible applications. *ISPRS Journal of Photogrammetry and Remote Sensing*, *168*, 74–88. https://doi.org/10.1016/j.isprsjprs.2020.07.021

Chakraborty, T., & Lee, X. (2019). A simplified urban-extent algorithm to characterize surface urban heat islands on a global scale and examine vegetation control on their spatiotemporal variability. *International Journal of Applied Earth Observation and Geoinformation*, *74*, 269–280. https://doi.org/10.1016/j.jag.2018.09.015

Chakraborty, T., Sarangi, C., & Lee, X. (2021). Reduction in human activity can enhance the urban heat island: Insights from the COVID-19 lockdown. *Environmental Research Letters*, *16*(5), 054060. https://doi.org/10.1088/1748-9326/abef8e

Chakraborty, T., Sarangi, C., & Tripathi, S. N. (2017). Understanding diurnality and inter-seasonality of a sub-tropical urban heat island. *Boundary-Layer Meteorology*, *163*(2), 287–309. https://doi.org/10.1007/s10546-016-0223-0

Chakraborty, T., Venter, Z., Lee, X., & Qian, Y. (2022). "*Netatmo Citizen Weather Station Data over Europe (July, 2019)*". Mendeley Data, V1. https://doi.org/10.17632/ck69zx89fc.1

Clinton, N., & Gong, P. (2013). MODIS detected surface urban heat islands and sinks: Global locations and controls. *Remote Sensing of Environment*, *134*, 294–304. https://doi.org/10.1016/j.rse.2013.03.008

Coffel, E. D., Horton, R. M., & De Sherbinin, A. (2017). Temperature and humidity based projections of a rapid rise in global heat stress exposure during the 21st century. *Environmental Research Letters*, *13*(1), 014001. https://doi.org/10.1088/1748-9326/aaa00e

Da Cunha, A. R. (2015). Evaluation of measurement errors of temperature and relative humidity from HOBO data logger under different conditions of exposure to solar radiation. *Environmental Monitoring and Assessment*, *187*(5), 1–11. https://doi.org/10.1007/s10661-015-4458-x

Du, H., Zhan, W., Liu, Z., Li, J., Li, L., Lai, J., et al. (2021). Simultaneous investigation of surface and canopy urban heat islands over global cities. *ISPRS Journal of Photogrammetry and Remote Sensing*, *181*, 67–83. https://doi.org/10.1016/j.isprsjprs.2021.09.003

Ebi, K. L., Capon, A., Berry, P., Broderick, C., de Dear, R., Havenith, G., et al. (2021). Hot weather and heat extremes: Health risks. *The Lancet*, *398*(10301), 698–708. https://doi.org/10.1016/S0140-6736(21)01208-3

ECA&D. (2013). *European Climate Assessment & Dataset (ECA&D)'Algorithm theoretical basis document (ATBD), version 10.7*. Royal Netherlands Meteorological Institute KNMI.

Fargione, J. E., Bassett, S., Boucher, T., Bridgham, S. D., Conant, R. T., Cook-Patton, S. C., et al. (2018). Natural climate solutions for the United States. *Science Advances*, *4*(11), eaat1869. https://doi.org/10.1126/sciadv.aat1869

Fong, K. C., Hart, J. E., & James, P. (2018). A review of epidemiologic studies on greenness and health: Updated literature through 2017. *Current Environmental Health Reports*, *5*(1), 77–87. https://doi.org/10.1007/s40572-018-0179-y

Gorelick, N., Hancher, M., Dixon, M., Ilyushchenko, S., Thau, D., & Moore, R. (2017). Google Earth Engine: Planetary-scale geospatial analysis for everyone. *Remote Sensing of Environment*, *202*, 18–27. https://doi.org/10.1016/j.rse.2017.06.031

Hardin, A. W., Liu, Y., Cao, G., & Vanos, J. K. (2018). Urban heat island intensity and spatial variability by synoptic weather type in the northeast US. *Urban Climate*, *24*, 747–762. https://doi.org/10.1016/j.uclim.2017.09.001

Heaviside, C., Macintyre, H., & Vardoulakis, S. (2017). The urban heat island: Implications for health in a changing environment. *Current Environmental Health Reports*, *4*(3), 296–305. https://doi.org/10.1007/s40572-017-0150-3

Heilig, G. K. (2014). *World urbanization prospects the 2014 revision*. United Nations, Department of Economic and Social Affairs (DESA), Population Division, Population Estimates and Projections Section.

Ho, H. C., Knudby, A., Xu, Y., Hodul, M., & Aminipouri, M. (2016). A comparison of urban heat islands mapped using skin temperature, air temperature, and apparent temperature (Humidex), for the greater Vancouver area. *Science of the Total Environment*, *544*, 929–938. https://doi.org/10.1016/j.scitotenv.2015.12.021

Hoffman, J. S., Shandas, V., & Pendleton, N. (2020). The effects of historical housing policies on resident exposure to intra-urban heat: A study of 108 US urban areas. *Climate*, *8*(1), 12. https://doi.org/10.3390/cli8010012

Howard, L. (1833). *The climate of London: Deduced from meteorological observations made in the metropolis and at various places around it* (Vol. 2). Harvey and Darton, J. and A. Arch, Longman, Hatchard, S. Highley [and] R. Hunter.

Hsu, A., Sheriff, G., Chakraborty, T., & Manya, D. (2021). Disproportionate exposure to urban heat island intensity across major US cities. *Nature Communications*, *12*(1), 2721. https://doi.org/10.1038/s41467-021-22799-5

Huang, K., Lee, X., Stone, B., Jr., Knievel, J., Bell, M. L., & Seto, K. C. (2021). Persistent increases in nighttime heat stress from urban expansion despite heat island mitigation. *Journal of Geophysical Research: Atmospheres*, *126*(4), e2020JD033831. https://doi.org/10.1029/2020jd033831

Hulley, G., Shivers, S., Wetherley, E., & Cudd, R. (2019). New ECOSTRESS and MODIS land surface temperature data reveal fine-scale heat vulnerability in cities: A case study for Los Angeles county, California. *Remote Sensing*, *11*(18), 2136. https://doi.org/10.3390/rs11182136

Jin, M., & Dickinson, R. E. (2010). Land surface skin temperature climatology: Benefitting from the strengths of satellite observations. *Environmental Research Letters*, *5*(4), 044004. https://doi.org/10.1088/1748-9326/5/4/044004

Keith, L., Meerow, S., & Wagner, T. (2019). Planning for extreme heat: A review. *Journal of Extreme Events*, *6*(03n04), 2050003. https://doi.org/10.1142/s2345737620500037

Krayenhoff, E. S., Broadbent, A. M., Zhao, L., Georgescu, M., Middel, A., Voogt, J. A., et al. (2021). Cooling hot cities: A systematic and critical review of the numerical modelling literature. *Environmental Research Letters*, *16*(5), 053007. https://doi.org/10.1088/1748-9326/abdcf1

Krayenhoff, E. S., Jiang, T., Christen, A., Martilli, A., Oke, T. R., Bailey, B. N., et al. (2020). A multi-layer urban canopy meteorological model with trees (BEP-Tree): Street tree impacts on pedestrian-level climate. *Urban Climate*, *32*, 100590. https://doi.org/10.1016/j.uclim.2020.100590

Laaidi, K., Zeghnoun, A., Dousset, B., Bretin, P., Vandentorren, S., Giraudet, E., & Beaudeau, P. (2012). The impact of heat islands on mortality in Paris during the August 2003 heat wave. *Environmental Health Perspectives*, *120*(2), 254–259. https://doi.org/10.1289/ehp.1103532

Li, D., Liao, W., Rigden, A. J., Liu, X., Wang, D., Malyshev, S., & Shevliakova, E. (2019). Urban heat island: Aerodynamics or imperviousness? *Science Advances*, *5*(4), eaau4299. https://doi.org/10.1126/sciadv.aau4299

Lokoshchenko, M. A. (2017). Urban heat island and urban dry island in Moscow and their centennial changes. *Journal of Applied Meteorology and Climatology*, *56*(10), 2729–2745. https://doi.org/10.1175/JAMC-D-16-0383.1

Maia-Silva, D., Kumar, R., & Nateghi, R. (2020). The critical role of humidity in modeling summer electricity demand across the United States. *Nature Communications*, *11*(1), 1686. https://doi.org/10.1038/s41467-020-15393-8

Maimaitiyiming, M., Ghulam, A., Tiyip, T., Pla, F., Latorre-Carmona, P., Halik, Ü., et al. (2014). Effects of green space spatial pattern on land surface temperature: Implications for sustainable urban planning and climate change adaptation. *ISPRS Journal of Photogrammetry and Remote Sensing*, *89*, 59–66. https://doi.org/10.1016/j.isprsjprs.2013.12.010

Manoli, G., Fatichi, S., Schläpfer, M., Yu, K., Crowther, T. W., Meili, N., et al. (2019). Magnitude of urban heat islands largely explained by climate and population. *Nature*, *573*(7772), 55–60. https://doi.org/10.1038/s41586-019-1512-9

Martilli, A., Krayenhoff, E. S., & Nazarian, N. (2020). Is the Urban Heat Island intensity relevant for heat mitigation studies? *Urban Climate*, *31*, 100541. https://doi.org/10.1016/j.uclim.2019.100541

Masterton, J. M., & Richardson, F. A. (1979). *Humidex: A method of quantifying human discomfort due to excessive heat and humidity*. Environment Canada, Atmospheric Environment.

Meier, F., Fenner, D., Grassmann, T., Otto, M., & Scherer, D. (2017). Crowdsourcing air temperature from citizen weather stations for urban climate research. *Urban Climate*, *19*, 170–191. https://doi.org/10.1016/j.uclim.2017.01.006

Meili, N., Manoli, G., Burlando, P., Bou-Zeid, E., Chow, W. T. L., Coutts, A. M., et al. (2020). An urban ecohydrological model to quantify the effect of vegetation on urban climate and hydrology (UT&C v1.0). *Geoscientific Model Development*, *13*(1), 335–362. https://doi.org/10.5194/gmd-13-335-2020

Mentaschi, L., Duveiller, G., Zulian, G., Corbane, C., Pesaresi, M., Maes, J., et al. (2022). Global long-term mapping of surface temperature shows intensified intra-city urban heat island extremes. *Global Environmental Change*, *72*, 102441. https://doi.org/10.1016/j.gloenvcha.2021.102441

Middel, A., Alkhaled, S., Schneider, F. A., Hagen, B., & Coseo, P. (2021). 50 Grades of shade. *Bulletin of the American Meteorological Society*, 1–35. https://doi.org/10.1175/BAMS-D-20-0193.1

Mishra, V., Ambika, A. K., Asoka, A., Aadhar, S., Buzan, J., Kumar, R., & Huber, M. (2020). Moist heat stress extremes in India enhanced by irrigation. *Nature Geoscience*, *13*(11), 722–728. https://doi.org/10.1038/s41561-020-00650-8

Muñoz-Sabater, J., Dutra, E., Agustí-Panareda, A., Albergel, C., Arduini, G., Balsamo, G., et al. (2021). ERA5-land: A state-of-the-art global reanalysis dataset for land applications [Preprint]. Data, Algorithms, and Models. https://doi.org/10.5194/essd-2021-82

Muller, C. L., Chapman, L., Grimmond, C. S. B., Young, D. T., & Cai, X. (2013). Sensors and the city: A review of urban meteorological networks: Sensors and the city. *International Journal of Climatology*, *33*(7), 1585–1600. https://doi.org/10.1002/joc.3678

Murage, P., Hajat, S., & Kovats, R. S. (2017). Effect of night-time temperatures on cause and age-specific mortality in London. *Environmental Epidemiology*, *1*, e005. https://doi.org/10.1097/EE9.0000000000000005

Napoly, A., Grassmann, T., Meier, F., & Fenner, D. (2018). Development and application of a statistically-based quality control for crowdsourced air temperature data. *Frontiers of Earth Science*, *6*, 118. https://doi.org/10.3389/feart.2018.00118

NASA Goddard Earth Sciences Data And Information Services Center. (2019). GPM IMERG final precipitation L3 1 day 0.1 degree x 0.1 degree V06 [Data set]. NASA Goddard Earth Sciences Data and Information Services Center. https://doi.org/10.5067/GPM/IMERGDF/DAY/06

Novick, K. A., & Katul, G. G. (2020). The duality of reforestation impacts on surface and air temperature. *Journal of Geophysical Research: Biogeosciences*, *125*(4), e2019JG005543. https://doi.org/10.1029/2019jg005543

Oleson, K. W., Monaghan, A., Wilhelmi, O., Barlage, M., Brunsell, N., Feddema, J., et al. (2015). Interactions between urbanization, heat stress, and climate change. *Climatic Change*, *129*(3), 525–541. https://doi.org/10.1007/s10584-013-0936-8

Paschalis, A., Chakraborty, T., Fatichi, S., Meili, N., & Manoli, G. (2021). Urban forests as main regulator of the evaporative cooling effect in cities. *AGU Advances*, *2*(2), e2020AV000303. https://doi.org/10.1029/2020AV000303

Perkins-Kirkpatrick, S. E., & Lewis, S. C. (2020). Increasing trends in regional heatwaves. *Nature Communications*, *11*(1), 3357. https://doi.org/10.1038/s41467-020-16970-7

Pesaresi, M., & Freire, S. (2016). GHS Settlement grid following the REGIO model 2014 in application to GHSL Landsat and CIESIN GPW v4-multitemporal (1975–1990–2000–2015). *JRC Data Cat*.

Qian, Y., Chakraborty, T. C., Li, J., Li, D., He, C., Sarangi, C., et al. (2022). Urbanization impact on regional climate and extreme weather: Current understanding, uncertainties, and future research directions. *Advances in Atmospheric Sciences*, *39*(6), 819–860. https://doi.org/10.1007/s00376-021-1371-9

Raymond, C., Matthews, T., & Horton, R. M. (2020). The emergence of heat and humidity too severe for human tolerance. *Science Advances*, *6*(19), eaaw1838. https://doi.org/10.1126/sciadv.aaw1838

Remme, R. P., Frumkin, H., Guerry, A. D., King, A. C., Mandle, L., Sarabu, C., et al. (2021). An ecosystem service perspective on urban nature, physical activity, and health. *Proceedings of the National Academy of Sciences*, *118*(22), e2018472118. https://doi.org/10.1073/pnas.2018472118

Rothfusz, L. P. (1990). *The heat index equation (or, more than you ever wanted to know about heat index)* (p. 9023). National Oceanic and Atmospheric Administration, National Weather Service, Office of Meteorology.

Rouse, J. W., Haas, R. H., Schell, J. A., Deering, D. W., & Harlan, J. C. (1974). *Monitoring the vernal advancement and retrogradation (green wave effect) of natural vegetation* (p. 371). NASA/GSFC Type III Final Report.

Sarangi, C., Qian, Y., Li, J., Leung, L. R., Chakraborty, T. C., & Liu, Y. (2021). Urbanization Amplifies nighttime heat stress on warmer days over the US. *Geophysical Research Letters*, *48*(24), e2021GL095678. https://doi.org/10.1029/2021GL095678

Schwaab, J., Meier, R., Mussetti, G., Seneviratne, S., Bürgi, C., & Davin, E. L. (2021). The role of urban trees in reducing land surface temperatures in European cities. *Nature Communications*, *12*(1), 1–11. https://doi.org/10.1038/s41467-021-26768-w

Sharma, A., Wuebbles, D. J., & Kotamarthi, R. (2021). The need for urban-resolving climate modeling across scales. *AGU Advances*, *2*(1), e2020AV000271. https://doi.org/10.1029/2020AV000271

Sherwood, S. C. (2018). How important is humidity in heat stress? *Journal of Geophysical Research: Atmospheres*, *123*(21), 11–808. https://doi.org/10.1029/2018JD028969

Sherwood, S. C., & Huber, M. (2010). An adaptability limit to climate change due to heat stress. *Proceedings of the National Academy of Sciences*, *107*(21), 9552–9555. https://doi.org/10.1073/pnas.0913352107

Steadman, R. G. (1979). The assessment of sultriness. Part I: A temperature-humidity index based on human physiology and clothing science. *Journal of Applied Meteorology and Climatology*, *18*(7), 861–873. https://doi.org/10.1175/1520-0450(1979)018<0861:taospi>2.0.co;2

Stone, B., Jr., Lanza, K., Mallen, E., Vargo, J., & Russell, A. (2019). Urban heat management in Louisville, Kentucky: A framework for climate adaptation planning. *Journal of Planning Education and Research*, 0739456X19879214. https://doi.org/10.1177/0739456X19879214

Stull, R. (2011). Wet-bulb temperature from relative humidity and air temperature. *Journal of Applied Meteorology and Climatology*, *50*(11), 2267–2269. https://doi.org/10.1175/JAMC-D-11-0143.1

Vargas, N. T., Chapman, C. L., Ji, W., Johnson, B. D., Gathercole, R., & Schlader, Z. J. (2020). Increased skin wetness independently augments cool-seeking behaviour during passive heat stress. *The Journal of Physiology*, *598*(13), 2775–2790. https://doi.org/10.1113/JP279537

Venter, Z. S., Chakraborty, T., & Lee, X. (2021). Crowdsourced air temperatures contrast satellite measures of the urban heat island and its mechanisms. *Science Advances*, *7*(22), eabb9569. https://doi.org/10.1126/sciadv.abb9569

Wan, Z. (2006). *MODIS land surface temperature products users' guide* (p. 805). Institute for Computational Earth System Science, University of California.

Wang, Z., Song, J., Chan, P. W., & Li, Y. (2021). The urban moisture island phenomenon and its mechanisms in a high-rise high-density city. *International Journal of Climatology*, *41*(S1), E150–E170. https://doi.org/10.1002/joc.6672

Wilcoxon, F., Kotz, S., & Johnson, N. L. (1992). *Breakthroughs in statistics: Methodology and distribution* (pp. 196–202). Springer New York.

Woetzel, J., Pinner, D., & Samandari, H. (2020). Climate risk and response: Physical hazards and socioeconomic impacts. https://www.mckinsey.com/~/media/McKinsey/Business%20Functions/Sustainability/Our%20Insights/Climate%20risk%20and%20response%20Physical%20hazards%20and%20socioeconomic%20impacts/MGI-Climate-risk-and-response-Executive-summary-vF.pdf

Wong, N. H., Tan, C. L., Kolokotsa, D. D., & Takebayashi, H. (2021). Greenery as a mitigation and adaptation strategy to urban heat. *Nature Reviews Earth & Environment*, *2*(3), 166–181. https://doi.org/10.1038/s43017-020-00129-5

Zhang, P., Bounoua, L., Imhoff, M. L., Wolfe, R. E., & Thome, K. (2014). Comparison of MODIS land surface temperature and air temperature over the continental USA meteorological stations. *Canadian Journal of Remote Sensing*, *40*(2), 110–122.

Zhao, L., Lee, X., & Schultz, N. M. (2017). A wedge strategy for mitigation of urban warming in future climate scenarios. *Atmospheric Chemistry and Physics*, *17*(14), 9067–9080. https://doi.org/10.5194/acp-17-9067-2017

Zhao, L., Lee, X., Smith, R. B., & Oleson, K. (2014). Strong contributions of local background climate to urban heat islands. *Nature*, *511*(7508), 216–219. https://doi.org/10.1038/nature13462

Zhao, L., Oleson, K., Bou-Zeid, E., Krayenhoff, E. S., Bray, A., Zhu, Q., et al. (2021). Global multi-model projections of local urban climates. *Nature Climate Change*, *11*(2), 152–157. https://doi.org/10.1038/s41558-020-00958-8

Zhao, Q., Yang, J., Wang, Z.-H., & Wentz, E. A. (2018). Assessing the cooling benefits of tree shade by an outdoor urban physical scale model at Tempe, AZ. *Urban Science*, *2*(1), 4. https://doi.org/10.3390/urbansci2010004

Zheng, Z., Zhao, L., & Oleson, K. W. (2021). Large model structural uncertainty in global projections of urban heat waves. *Nature Communications*, *12*(1), 1–9. https://doi.org/10.1038/s41467-021-24113-9

Zhou, D., Xiao, J., Bonafoni, S., Berger, C., Deilami, K., Zhou, Y., et al. (2018). Satellite remote sensing of surface urban heat islands: Progress, challenges, and perspectives. *Remote Sensing*, *11*(1), 48. https://doi.org/10.3390/rs11010048

Ziter, C. D., Pedersen, E. J., Kucharik, C. J., & Turner, M. G. (2019). Scale-dependent interactions between tree canopy cover and impervious surfaces reduce daytime urban heat during summer. *Proceedings of the National Academy of Sciences*, *116*(15), 7575–7580. https://doi.org/10.1073/pnas.1817561116